PCCP

Accepted Manuscript

ROYAL SOCIETY OF CHEMISTRY

www.rsc.org/pccp

Physical Chemistry Chemical Physics RSCPublishing

COMMUNICATION

Anomalous Low-Temperature Proton Conductivity Enhancement in a Novel Protonic Nanocomposite

Cite this: DOI: 10.1039/x0xx00000x

D. Clark,[a] J. Tong,[a*] A. Morrissey,[a] A. Almansoori,[b] I. Reimanis[a] and R. O'Hayre[a*]

Received ooth January 2012,
Accepted ooth January 2012

DOI: 10.1039/x0xx00000x

www.rsc.org/

A novel protonic ceramic composite is synthesized that comprises nanoscale nickel metal films partially decorating the grain boundaries of the proton-conducting ceramic, $BaCe_{0.7}Zr_{0.1}Y_{0.1}Yb_{0.1}O_{3-\delta}$ (BCZYYb). Low-temperature proton conductivity improvements of up to 46X vs. a control are observed, suggesting a novel method to enhance ion conductivity in polycrystalline materials.

Proton conducting ceramics show significant proton conductivity in wet or reducing atmospheres, making them suitable for applications in protonic ceramic fuel cells (PCFCs), permeation membranes, electrolyzers, membrane reactors, and hydrogen sensors.[1] Recently it has been reported that the composition $BaCe_{0.7}Zr_{0.1}Y_{0.1}Yb_{0.1}O_{3-\delta}$ (BCZYYb) shows excellent ionic (protonic) conductivity at temperatures as low as 500 °C in addition to sulfur poisoning and coking resistance which is crucial for the above applications.[2] Under these lower-temperature conditions, BCZYYb attains much higher conductivity than traditional solid electrolytes such as yttria-stabilized zirconia (YSZ; oxygen ion conductor), $BaZr_{0.8}Y_{0.2}O_{3-\delta}$ (BZY20; proton conductor), $Ce_{0.9}Gd_{0.1}O_{1.95}$ (GDC; oxygen ion conductor), or $La_{0.9}Sr_{0.1}Ga_{0.9}Mg_{0.1}O_{3-\delta}$ (LSGM; oxygen ion conductor).[2-4] Nevertheless, as with most ceramic ion conductors, the low-temperature ionic conductivity in BCZYYb is limited by highly resistive grain boundaries.[1,5]

The recognition that interfaces can dominate ionic behavior has long been appreciated in the solid-state ionics community. The study and manipulation of interfacial ionic phenomena, dubbed "nanoionics," is now being intensively pursued.[6] Nanoionic effects have been particularly widely explored and exploited in carefully engineered ceramic/ceramic heterostructures. As a well-known example, CaF_2/BaF_2 multilayer stacks show a dramatic enhancement in fluorine ion conductivity by up to three orders of magnitude, with conductivity increasing as the interfacial area begins to dominate at smaller layer thicknesses.[7,8] In addition to heterogeneous interfaces, homogeneous interfaces (e.g. grain boundaries) can also strongly alter the ionic transport properties of materials. Recently, anomalous low-temperature (< 350 °C) proton conduction has been demonstrated in otherwise non-proton conducting materials upon nanostructuring. Maglia, et al. have shown proton conductivity in humid oxygen atmospheres in nanocrystalline TiO_2 prepared by high pressure field-assisted sintering;[9] similarly, anomalous low-temperature proton conduction behavior has also been observed in nanocrystalline yttria-stabilized zirconia (YSZ).[10,11] It is believed that the cause of this phenomenon is a percolating absorbed water-film region which arises due to nanoporosity along the grain boundaries that dictate the proton transport.

Despite the widespread studies of nanoionic and nanometric phenomena in a variety of homogeneous and heterogeneous systems, there are few studies of such nanoionic phenomena in ceramic/metallic heterostructures. In this paper, we demonstrate a novel, inexpensive method to partially modify the grain boundaries of BCZYYb with thin metal films to increase protonic conductivity. Because the metal film modification is only partial, percolating electrical conductivity is not induced. However, the modification results in a significant enhancement in the low-temperature proton conductivity under wet reducing conditions by significantly suppressing the grain boundary resistance of the system. Detailed analysis of the conductivity response with electrochemical impedance spectroscopy (EIS), concentration cell measurements, and isotope experiments confirms that the conduction enhancement is protonic and provides insights into the potential mechanism of enhancement, thereby highlighting the potential of using metallic-modification of grain boundaries as a new strategy to enhance ionic conductivity in crystalline ceramic conductors.

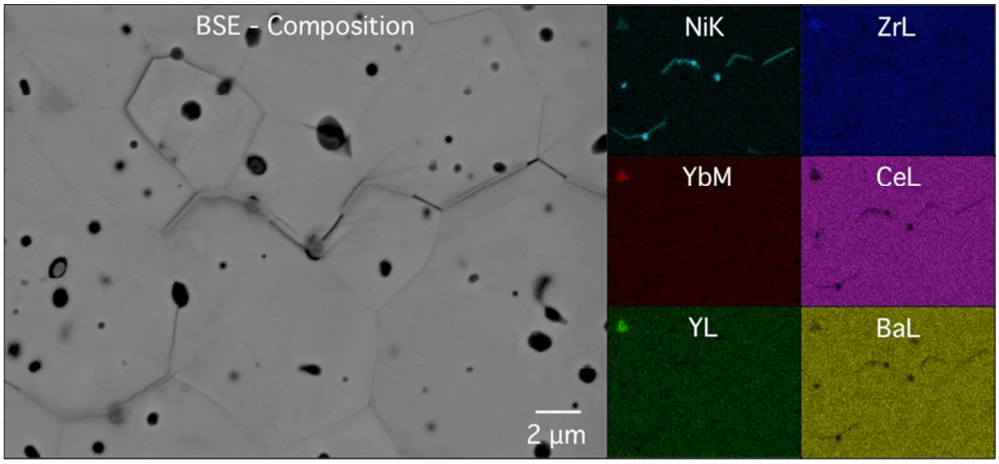

Fig. 1 Energy dispersive x-ray spectroscopy (EDS) map of a polished cross-section of BCZYYb/Ni post-reduction showing nickel at the grain boundaries. Reduced at 750 °C for 48 h in 5% H_2. Large image showing compositional backscatter electron image and corresponding elemental maps of Ni, Zr, Yb, Ce, Y, and Ba (and their x-ray peak K, L, or M). The brighter the pixel, the higher the concentration (dark represents depletion).

Nickel interfaces were created along the grain boundaries of sintered polycrystalline BCZYYb pellets using solid-state reactive sintering (SSRS) with 1.0 wt. % NiO added[12,13] by an in-situ internal reduction process[14,15] using wet (~3% H_2O) 5% H_2 for 48 h. Nickel was chosen because of its compatibility with the BCZYYb system. Under oxidizing conditions, NiO is soluble in barium cerate/zirconate perovskite ceramics up to at least 1 wt. % (~4-5 mol %) without second-phase formation. Under reducing conditions, it can then be exsolved from the perovskite lattice as metallic nickel. Fig. 1 shows energy dispersive x-ray spectroscopy (EDS) maps with the corresponding backscatter SEM image illustrating the presence of nickel regions along some of the grain boundaries of the reduced ceramic. It can also be seen that there is some minor grain boundary cracking within the material (possibly induced post-polishing). The presence of these nickel regions was not found in the BCZYYbNiO1 before reduction (Fig. S1). These regions are shown in greater detail in Fig. 2 with TEM bright-field images of the nickel regions at the grain boundaries in the reduced BCZYYbNiO1 (hereafter referred to as BCZYYb/Ni). 60 – 100 nm nickel metal films form along select grain boundaries.

SQUID magnetometry (Fig. S2), which can differentiate between Ni^{2+} in solid solution, NiO, and Ni metal, was performed on an as-sintered pellet, as well as a reduced pellet (5% H_2 bal. Ar for 48 h), and a pellet that had been subjected to conductivity measurement (~400 h reduction in 5% H_2 bal. Ar at different temperatures). These magnetic measurements show that before reduction (as-sintered), only Ni^{2+} ions were present in solid solution, while after reduction 71 ± 7% of the nickel had been reduced to Ni metal (the remainder stayed as Ni^{2+}; no NiO was found via magnetometry for any of the samples). The sample subjected to conductivity measurement showed 65 ± 7% of the nickel as nickel metal, indicating negligible differences in reduction amount after long-term testing under reducing conditions as compared to the initial 48 h reduction. Because 1.0 wt. % (~4.1 atomic %) NiO was added during synthesis, and magnetometry indicates that ~70% of it was converted to nickel metal upon reduction, the resulting volume of nickel metal within the reduced BCZYYb/Ni composite is ~0.3 vol.%. This volume estimate from magnetometry agrees well with an SEM estimate of 0.2 – 0.25 vol.% Ni metal calculated based on the measured grain size (~8 µm) and the observation that ~30 - 40 % of grain boundaries (rough estimate from SEM cross-sections and EDS maps) are coated by 60 - 100 nm thick nickel metal layers. Therefore, almost all of the original nickel has been accounted for, existing as either Ni^{2+} in solid solution or as nickel metal along the grain boundaries.

Total conductivities of the BCZYYb/Ni protonic nanocomposite and BCZYYb control (BCZYYb-C) under both dry reducing (Fig. 3A) conditions (5% H_2 bal. Ar) and wet (~3% H_2O) reducing (Fig. 3B) conditions were assessed by EIS. Under dry reducing conditions, the conductivity of the two pellets is similar, although the control sample shows slightly higher conductivity (~15 - 30%) than the BCZYYb/Ni nanocomposite over most of the temperature range. Both also show two distinct conduction regimes, with a low-energy slope (~0.35 eV for both) from 750 – 350 °C and a high-energy slope (~0.72 - 0.83 eV) from 350 – 100 °C. We attribute the high-temperature activation energy to bulk proton transport, which is consistent with the literature reports

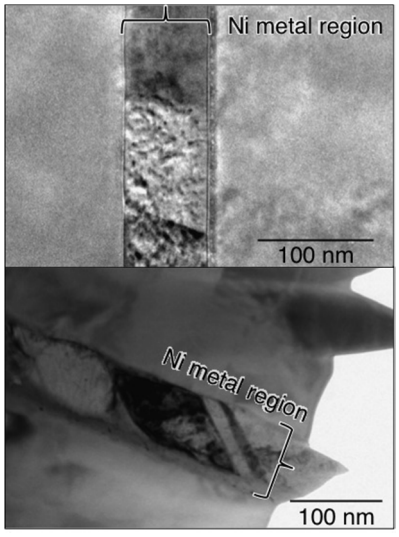

Fig. 2 Bright-field TEM images of nickel metal regions at BCZYYb grain boundaries after reduction. Reduced at 750 °C for 48 h in 5% H_2. Some twinning is observed in the nickel regions. Nickel metal films were not found at every grain boundary.

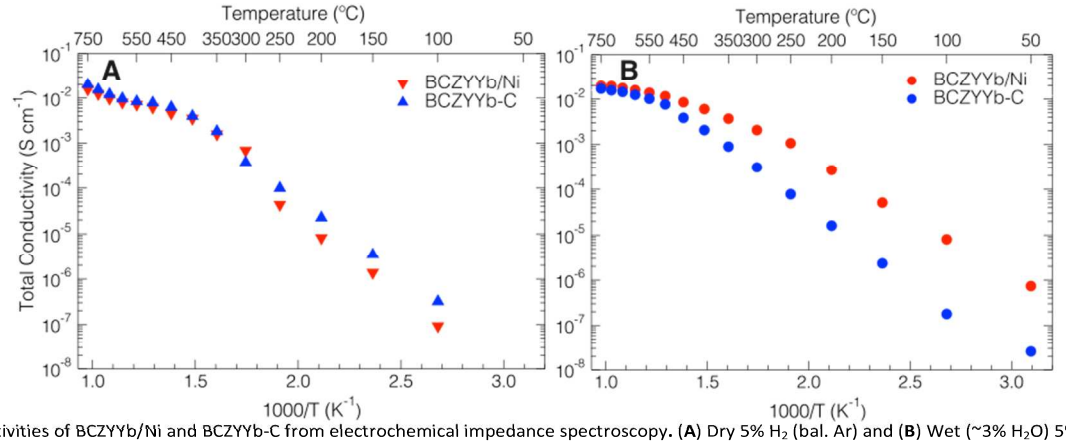

Fig. 3 Total conductivities of BCZYYb/Ni and BCZYYb-C from electrochemical impedance spectroscopy. (**A**) Dry 5% H_2 (bal. Ar) and (**B**) Wet (~3% H_2O) 5% H_2 (bal. Ar).

of BZY and BCY,[1,5] while the low-temperature activation energy corresponds to what is expected for grain-boundary dominated proton transport.[1,5,16,17]

In contrast to the dry reducing conditions, under wet reducing conditions (more relevant to most technological applications) the BCZYYb/Ni nanocomposite shows enhanced conductivity relative to the control throughout the entire temperature range (750 - 50 °C). For temperatures over 550 °C, an enhancement of 15 - 27% over the control sample is observed. This is attributed to the increase in oxygen vacancies ($VO^{\bullet\bullet}$) due to the aliovalent substitution of Ni^{2+} in solid solution on the Zr^{4+} (or Ce^{4+}) site, as shown in eqn (1).

$$1/2O_2 + NiO \rightarrow Ni'_{Zr} + V_O^{\bullet\bullet} + 2O_O^{\times} \quad (1)$$

In this temperature range, both samples show total conductivities broadly consistent with previous literature reports. However, as the temperature decreases, the degree of conductivity enhancement in the BCZYYb/Ni nanocomposite increases dramatically, resulting in >10X enhancement for temperatures under 250 °C (enhancement of 46X at 100 °C). While significant enhancements in low-temperature conductivity under wet reducing conditions have been previously observed in nanocrystalline oxides,[18-23] the enhancement in this case is quite unprecedented given the fact that the BCZYYb/Ni composite is a dense, large-grained (~8 μm grain size) bulk ceramic. Furthermore, the control sample (BCZYYb-C), which has smaller grain size (~3 μm), does not manifest this low-temperature conductivity enhancement.

While the conductivity response of the control pellet under wet reducing conditions can still be separated into two temperature regimes with two distinct slopes (with activation energies that are similar to the behavior under dry reducing conditions), the BCZYYb/Ni nanocomposite pellet shows a changing slope until temperatures below 250 °C. This changing slope at higher temperatures suggests a transition in the transport mechanisms as the temperature decreases. The single slope region from 250 – 50 °C yields an activation energy of 0.56 eV. This region's activation energy is 0.11 eV lower than the control pellet's activation energy at the same temperature (0.67 eV), suggesting that a different conduction mechanism may dominate in the BCZYYb/Ni nanocomposite sample at lower temperatures under wet reducing conditions. The enhancement may be due to a space-charge effect arising from the contact between the higher work function nickel metal with the lower-work function BCZYYb. Additionally, it is also possible that protons from the ceramic may be soluble, and mobile, in the nickel metal itself, as Ni is a well-known hydrogen permeable material. Another possibility is the formation of a water film at the nanoporous regions at the Ni/BCZYYb interfaces, similar to what has been seen with other ion conductors at low temperatures.[9-11] The dramatic difference in dry versus wet behavior for the composite pellet could indicate the carrier concentration is too low under dry conditions to be sensitive to the enhancement from the BCZYYb/Ni regions. Since Wagner hydration, shown in eqn (2), is important for proton incorporation in these materials,[5] it is expected

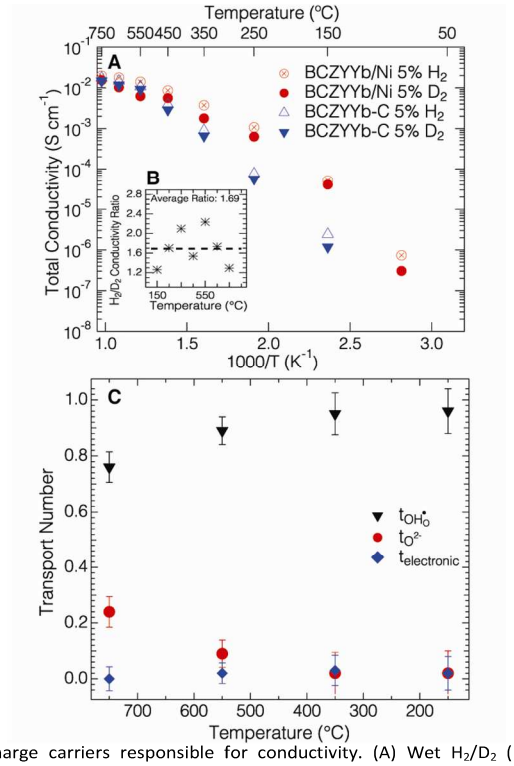

Fig. 4 Charge carriers responsible for conductivity. (A) Wet H_2/D_2 (H_2O/D_2O) isotope conductivities of BCZYYb/Ni and BCZYYb-C from 750 – 50 °C. (B) The ratio of D_2 to H_2 conductivity for BCZYYb/Ni for the given temperatures plotted with the average ratio (1.4 shows isotopic effect). (C) Transport numbers for protons, oxygen-ions, and electrons/holes (electronic) for BCZYYb/Ni measured via a concentration cell by varying pH_2 and pH_2O gradient around 5% H_2 (bal. Ar).

that the concentration of protons may be higher in the BCZYYb/Ni sample due to the increased oxygen vacancy concentration in this sample caused by the Ni^{2+} defect reaction in eqn (1). In a dry environment the conductivity increase is not observed, due to low carrier concentrations.

$$H_2O+V_O^{\bullet\bullet} \rightarrow 2OH_O^{\bullet} \quad (2)$$

This also explains the changes in activation energies from dry to wet environments for both BCZYYb-C and BCZYYb/Ni.

In order to further investigate the origins of the enhancement phenomena, the conductivities were separated and normalized into grain boundary and bulk contributions (Fig. S3) using the standard brick-layer impedance model (see Supplementary Materials for details on the analysis).[24-26] An examination of the specific bulk and grain boundary conductivities shows that the bulk and grain boundary conductivities for the BCZYYb/Ni sample are modestly lower than the bulk and grain boundary conductivities for the BCZYYb-C in the dry reducing environment. In the wet reducing environment, the bulk and grain boundary contributions could not be separated for the BCZYYb/Ni sample because of the significantly lower impedance. However, the much higher overall conductivity of the BCZYYb/Ni compared to the BCZYYb-C under wet reducing conditions, especially at lower temperatures where the grain boundary contribution typically dominates, suggests that the improved performance is most likely due to a substantial increase in the grain boundary conductivity for the BCZYYb/Ni under these conditions.

To assess whether electronic conduction could be responsible for the enhanced low-temperature conductivity of the BCZYYb/Ni nanocomposite sample under wet reducing conditions, isotope and concentration cell measurements were conducted. Isotope experiment results in Fig. 4A and 4B show a clear H/D isotopic effect throughout the entire temperature range with an average ratio (H^+ conductivity/D^+ conductivity) of 1.69 ± 0.37 for BCZYYb/Ni and 1.40 ± 0.31 for the BCZYYb-C, demonstrating that both materials are dominantly proton conducting, even at low temperatures, and therefore that the observed low-temperature conductivity enhancement in the BCZYYb/Ni sample is likely protonic in origin. Furthermore, the isotope measurements, although carried out on a different pellet than the conductivity measurement, showed less than 7% error (almost indistinguishable on a log plot) from the initial conductivity measurements shown in Fig. 3A, indicating reproducibility of the conductivity enhancement effect.

In order to further quantify the ionic vs. electronic transport, concentration cell measurements were completed on the BCZYYb/Ni composite pellet (Fig. 4C). Electronic conductivity is negligible in the BCZYYb/Ni composite at all temperatures. The proton transport number is greater than 0.95 at low temperatures, and decreases only at high temperatures where oxygen ion conduction begins to contribute.

Conclusions

In summary, 60 – 100 nm thick nickel metal layers were created at select grain boundaries of SSRS-produced BCZYYbNiO1 upon reduction. These BCZYYb/Ni composites showed a remarkable order-of-magnitude enhancement in proton conductivity above the control at temperatures below 450 °C in wet reducing conditions (with up to a 46X enhancement seen at 100 °C, about 3-5X higher than the previous highest values obtained in the literature).[27-33] In dry reducing conditions, this enhancement was not observed. While the mechanism of the enhancement is as-yet unclear, we speculate that it could be caused by an increased concentration of charge carriers in or around the nickel metal regions at the grain boundaries, due to the mismatch in work function at the interface.[6,34,35] While it is uncommon to report conductivities below 400 °C in these materials as they are generally too low for device applications, this composite demonstrates the highest total (bulk + grain boundary) proton conductivity reported for a polycrystalline perovskite at low-temperatures (Fig. S4).[1-3,27-33] Since the Ni metal stability relies on a reducing environment, these enhancements may only be relevant to H_2 sensing/separation applications or protonic membrane reactors for applications such as gas-to-liquid (GTL) fuel synthesis. The work therefore demonstrates the principle of using metallic-modification of grain boundaries as a new strategy to enhance ionic conductivity in crystalline ceramic conductors, and with further optimization, could open the door to the specific application of metal-modified ceramic proton conductors at temperatures below 400 °C.

Acknowledgments

This work has been supported by The Petroleum Institute in Abu Dhabi, UAE, the National Science Foundation MRSEC program under Grant No. DMR-0820518, the National Science Foundation Graduate Research Fellowship under Grant No. DGE-1057607, and by the National Science Foundation Ceramics Program under Grant No. DMR-1003030 at the Colorado School of Mines. We acknowledge the use of magnetometry facilities in the Magnetics Group at the National Institute for Standards and Technology in Boulder, Colorado.

Notes and references

[a] Department of Metallurgical and Materials Engineering, Colorado School of Mines, Golden, CO 80401, USA.
[b] Department of Chemical Engineering, The Petroleum Institute, Abu Dhabi, UAE.

Electronic Supplementary Information (ESI) available: Materials and methods with supplementary figures. See DOI: 10.1039/c000000x/

1 K. D. Kreuer, *Annu. Rev. Mater. Res.*, 2003, **33**, 333–359.
2 L. Yang, S. Z. Wang, K. Blinn, M. F. Liu, Z. Liu, Z. Cheng, and M. Liu, *Science*, 2009, **326**, 126–129.
3 F. Zhao, C. Jin, C. Yang, S. Wang, and F. Chen, *J. Power Sources*, 2011, **196**, 688–691.
4 T. Ishihara, H. Matsuda, and Y. Takita, *J. Am. Chem. Soc.*, 1994, **116**, 3801–3803.
5 K. D. Kreuer, *Solid State Ionics*, 1999, **125**, 285–302.
6 J. Maier, *Nat. Mater.*, 2005, **4**, 805–815.
7 N. Sata, K. Eberman, K. Eberl, and J. Maier, *Nature*, 2000, **408**, 946–949.
8 X. Guo and J. Maier, *Adv. Funct. Mater.*, 2009, **19**, 96–101.

9 F. Maglia, I. G. Tredici, G. Spinolo, and U. Anselmi-Tamburini, *J. Mater. Res.*, 2012, **27**, 1975–1981.
10 U. Anselmi-Tamburini, F. Maglia, G. Chiodelli, P. Riello, S. Bucella, and Z. a. Munir, *Appl. Phys. Lett.*, 2006, **89**, 163116.
11 G. Chiodelli, F. Maglia, U. Anselmi-Tamburini, and Z. a. Munir, *Solid State Ionics*, 2009, **180**, 297–301.
12 J. H. Tong, D. Clark, M. Hoban, and R. O'Hayre, *Solid State Ionics*, 2010, **181**, 496–503.
13 Y. Liu, L. Yang, M. M. Liu, and Z. Tang, *J. Power Sources*, 2011, **196**, 9980–9984.
14 J. T. White, I. E. Reimanis, J. Tong, J. R. O'Brien, and A. Morrissey, *J. Am. Ceram. Soc.*, 2012, **95**, 4008–4014.
15 H. Schmalzried and M. Backhaus-Ricoult, *Prog. Solid State Chem.*, 1993, **22**, 1–57.
16 K. Katahira, Y. Kohchi, T. Shimura, and H. Iwahara, *Solid State Ionics*, 2000, **138**, 91–98.
17 T. Scherban, W. K. Lee, and A. S. Nowick, *Solid State Ionics*, 1988, **28-30**, 585–588.
18 I. Kosacki, V. Petrovsky, and H. U. Anderson, *Appl. Phys. Lett.*, 1999, **74**, 341–343.
19 A. Karthikeyan, C.-L. Chang, and S. Ramanathan, *Appl. Phys. Lett.*, 2006, **89**, 183113–183116.
20 Y. M. Chiang, E. B. Lavik, and D. A. Blom, *Nanostructured Mater.*, 1997, **9**, 633–642.
21 Y. M. Chiang, E. B. Lavik, I. Kosacki, H. L. Tuller, and J. Y. Ying, *Appl. Phys. Lett.*, 1996, **69**, 185–187.
22 S. Kim and J. Maier, *J. Electrochem. Soc.*, 2002, **149**, J73–J83.
23 I. Kosacki and H. U. Anderson, *Sensors Actuators B Chem.*, 1998, **48**, 263–269.
24 N. M. Beekmans and L. Heyne, *Electrochim. Acta*, 1976, **21**, 303–310.
25 S. M. Haile, D. L. West, and J. Campbell, *J. Mater. Res.*, 1998, **13**, 1576–1595.
26 H. Nafe, *Solid State Ionics*, 1984, **13**, 255–263.
27 Y. Yamazaki, R. Hernandez-Sanchez, and S. M. Haile, *Chem. Mater.*, 2009, **21**, 2755–2762.
28 Y. Yamazaki, R. Hernandez-Sanchez, and S. M. Haile, *J. Mater. Chem.*, 2010, **20**, 8158–8166.
29 I. Ahmed, S. M. H. Rahman, P. Steegstra, S. T. Norberg, S.-G. Eriksson, E. Ahlberg, C. S. Knee, and S. Hull, *Int. J. Hydrogen Energy*, 2010, **35**, 6381–6391.
30 P. Babilo and S. M. Haile, *J. Am. Ceram. Soc.*, 2005, **88**, 2362–2368.
31 H. Iwahara, T. Esaka, H. Uchida, and N. Maeda, *Solid State Ionics*, 1981, **3-4**, 359–363.
32 P. Babilo, T. Uda, and S. M. Haile, *J. Mater. Res.*, 2007, **22**, 1322–1330.
33 H. Iwahara, H. Uchida, K. Ono, and K. Ogaki, *J. Electrochem. Soc.*, 1988, **135**, 529.
34 J. Maier, *Phys. Chem. Chem. Phys.*, 2009, **11**, 3011–3022.
35 H. Matsumoto, Y. Furya, S. Okada, T. Tanji, and T. Ishihara, *Electrochem. Solid-State Lett.*, 2007, **10**, P11–P13.
36

Graphical Abstract

A novel protonic ceramic composite is synthesized that comprises nanoscale nickel metal films the grain boundaries of the proton-conducting ceramic, $BaCe_{0.7}Zr_{0.1}Y_{0.1}Yb_{0.1}O_{3-\delta}$. Low-temperature proton conductivity improvements of up to 46X are observed.